Published in final edited form as:
Osteoarthritis Cartilage. 2011 July ; 19(7): 864–873. doi:10.1016/j.joca.2011.04.011.

Acute Joint Pathology and Synovial Inflammation is Associated with Increased Intra-Articular Fracture Severity in the Mouse Knee

John S. Lewis Jr.[*], **W. Chad Hembree**[*], **Bridgette D. Furman**, **Lauren Tippets**, **Dennis Cattel**, **Janet L. Huebner**, **Dianne Little**, **Louis E. DeFrate**, **Virginia B. Kraus**, **Farshid Guilak**, and **Steven A. Olson**
Department of Orthopaedic Surgery, Duke University Medical Center, Durham, NC 27710

Abstract

OBJECTIVE—Post-traumatic arthritis is a frequent cause of disability and occurs most commonly and predictably after articular fracture. The objective of this investigation was to examine the effect of fracture severity on acute joint pathology in a novel murine model of intra-articular fracture.

DESIGN—Low and high energy articular fractures (n=25 per group) of the tibial plateau were created in adult male C57BL/6 mice. The acute effect of articular fracture severity on synovial inflammation, bone morphology, liberated fracture area, cartilage pathology, chondrocyte viability, and systemic cytokines and biomarkers levels was assessed at 0, 1, 3, 5, and 7 days post-fracture.

RESULTS—Increasing intra-articular fracture severity was associated with greater acute pathology in the synovium and bone compared to control limbs, including increased global synovitis and reduced periarticular bone density and thickness. Applied fracture energy was significantly correlated with degree of liberated cortical bone surface area, indicating greater comminution. Serum concentrations of hyaluronic acid (HA) were significantly increased one day post-fracture. While articular fracture significantly reduced chondrocyte viability, there was no relationship between fracture severity and chondrocyte viability, cartilage degeneration, or systemic levels of cytokines and biomarkers.

CONCLUSIONS—This study demonstrates that articular fracture is associated with a loss of chondrocyte viability and increased levels of systemic biomarkers, and that increased intra-articular fracture severity is associated with increased acute joint pathology in a variety of joint tissues, including synovial inflammation, cortical comminution, and bone morphology. Further characterization of the early events following articular fracture could aid in the treatment of post-traumatic arthritis.

Keywords

cartilage; osteoarthritis; trauma; intra-articular fracture; synovium; inflammation

Corresponding author: Steven A. Olson, M.D., Duke University Medical Center, Box 3389, Durham, NC 27710, Tel (919) 668-3000, Fax (919) 668-2933, olson016@mc.duke.edu.
[*]These authors contributed equally to this manuscript and share first authorship.

Contributions: Conception and study design: SAO, FG, BDF; Collection and assembly of data: JSL, WCH, BDF, LT, DC, JLH, DL; Analysis of data: JSL, WCH, BDF, LT, DC, LED; Interpretation of data: JSL, WCH, BDF, LT, DC, JLH, DL, LED, VBK, FG, SAO; Drafting the article: JSL, WCH; Critical revision of the article: SAO, FG, BDF, JLH, DL, LED, VBK; Final approval of the version to be submitted: JSL, WCH, BDF, LT, DC, JLH, DL, LED, VBK, FG, SAO.

Conflict of interest: The authors declare no conflict of interest.

INTRODUCTION

Post-traumatic arthritis (PTA) is a frequent cause of disability following trauma of weight-bearing joints, and it is estimated that 12% of the nearly 21 million Americans with symptomatic osteoarthritis (OA) have a post-traumatic etiology [1, 2]. PTA can develop after a variety of joint injuries but occurs commonly after intra-articular fracture [2]. Importantly, more severe fractures, characterized by greater displacement of the articular surface and subchondral bone and greater degree of comminution, have a worse prognosis [3]. Thus energy of injury and subsequent intra-articular fracture severity may play a fundamental role in the pathologic progression of PTA and also serve as an important prognostic indicator for clinical outcomes [3, 4].

While various types of joint trauma can cause PTA, the mechanisms by which the extent of injury severity may lead to increased joint degeneration is unclear [5-10]. Loss of chondrocyte viability following traumatic impact at the time of intra-articular fracture may contribute to PTA [11, 12]. Cell death and altered cartilage structure can be present in a traumatized joint in the absence of articular fracture [13-16]. Injuries severe enough to result in intra-articular fracture, however, undoubtedly involve cell death and altered cartilage structure as well [17, 18]. Pro-inflammatory cytokines such as IL-1 and TNF-α are up-regulated in injured and degenerative joints and may play an important role in the pathogenesis of PTA [19, 20]. The effect of articular fracture on synovial inflammation remains unknown, although synovial pathology is critical in the development of various forms of arthritis [21, 22].

The objective of this study was to examine the effect of intra-articular fracture severity on acute pathology within various joint tissues in a murine model of closed articular fracture that results in progressive osteoarthritic changes in bone and articular cartilage following a single periarticular injurious load [23]. We hypothesized that increased energy of fracture would lead to increased intra-articular fracture severity, which would be reflected in quantitative measures of increased liberated cortical bone surface area (indicating greater comminution). Furthermore, we examined the hypothesis that increased fracture severity would be associated with acute increases in synovial pathology, bone morphological changes, chondrocyte death, degeneration of the articular cartilage, and levels of circulating inflammatory cytokines and biomarkers.

METHODS

All procedures were performed in accordance with protocols approved by the Duke University Institutional Animal Care and Use Committee. Fifty-six mice (male, C57BL/6, 8wks) were obtained from Charles River Laboratories. Animals were housed until 16 weeks of age, at which time active growth has decreased, and peak bone mass is achieved [24, 25]. As described previously [23], animals were anesthetized (pentabarbitol, i.p.60mg/kg) and placed in a custom cradle with the left hindlimb in neutral position (90° flexion). A custom indenter applied a 10N pre-load to the anterior aspect of the left proximal tibial plateau, followed by compression applied at a rate of 20N/s. Two different loads were applied: a low energy fracture, with a displacement limit of 3.2mm, and a high energy fracture, with no limit on displacement. The energy of fracture was calculated from load-displacement curves for each joint. Group one (n=25) was subjected to low energy fractures. Group two (n=25) was subjected to high energy. Additional mice were utilized as non-fractured controls (n=3) or shams (knee probed, fracture load omitted; n=3).

All mice underwent high resolution digital radiographs (Model MX-20 Digital, Faxitron) within 1hr to confirm the presence of an articular fracture. No fixation or surgical intervention was employed. Animals were given analgesic (buprenorphine, s.q. 0.1mg/kg, bid) for 48hrs following fracture inductions and allowed immediate ad libitum weight bearing and motion. Mice were sacrificed at 0(n=8), 1(n=3), 3(n=3), 5(n=3), and 7(n=8) days post-fracture per group. Contralateral limbs were used as controls unless otherwise indicated. Non-fractured controls were sacrificed at day 0, and sham animals were sacrificed at day 7.

To determine chondrocyte viability, hind limbs from 3 randomly selected animals per group from all timepoints were excised, overlying skin and musculature carefully removed, and capsulectomy performed. Confocal microscopy with a fluorescent live/dead assay was initially attempted, but complications due to the small size and instability of multiple osteochondral fragments in the fractured mouse joint forced us to abandon this methodology. As an alternative, chondrocyte viability was assessed using nitroblue tetrazolium (NBT). NBT is cell-permeable and metabolized by live cells to form a blue formazan product which remains stable to standard histological preparation and paraffin-embedding. Various studies have documented NBT as a live cell marker for chondrocytes [26, 27]. Because an alternative method of assessing chondrocyte viability was used, shams were also assessed. For NBT analysis, limbs were incubated (5% CO_2, 37°C) for 24hrs in 6ml of solution containing 1.5mg/ml NBT in Ham's F12, 5% FBS, and 1% penicillin/streptomycin. Limbs were then fixed in 10% buffered formalin in a neutral position of the limb (90° flexion) for microCT evaluation followed by histology.

A modified grading scale was used to qualitatively assess the percentage of live cells in the cartilage for those limbs stained with NBT (Table 1). First, the central region of the joint was identified on coronal histologic sections by the presence of the anterior cruciate ligament and triangular shaped sections of both the medial and lateral menisci. An additional section was chosen from an anterior region located 120 to 200μm anterior to the first section. The medial and lateral femoral condyles, and medial and lateral aspects of the tibial plateau were graded separately by 4 blinded graders *(maximum site score 5)* and then summed to calculate a total joint score *(maximum score 20)* for each joint. An increasing score was associated with increased chondrocyte death.

All hind limbs at 0 and 7 days post-fracture were scanned by a desktop microCT system (microCT 40, Scanco Medical AG, Bassersdorf, Switzerland). A hydroxyapatite calibration phantom was used to calibrate bone density values (mg/cm^3). Morphometric bone parameters were determined in the distal femoral condyles, proximal tibial plateau immediately distal to subchondral bone, and metaphyseal region of tibia, as previously described [23]. Parameters reported in the femoral condyles were trabecular bone fraction (bone volume/total volume) and bone density (mg/cm^3). Parameters reported in the tibial plateau and metaphyseal regions include bone volume (mm^3) and bone density (mg/cm^3). Subchondral bone thickness was also measured in the central region of the joint, as previously described [23].

Fractures were characterized for degree of comminution by measuring liberated surface area [4] from microCT images in a subset of animals from both low and high energy fractures (n=8). Semi-automated edge detection software employing a Canny filter (Mathematica 6.0, Wolfram, Champaign, IL) was used to outline cortical bone in axial CT scans with a voxel size of 16×16×16μm. Spline curves were used to segment the edges of cortical bone within each image and to create a 3D model of each joint. The fractured joint 3D model was then aligned with its contralateral control using an iterative closest point technique [28], and the change in surface area between the two models was calculated. The liberated surface area

was then plotted as a function of applied fracture energy [4]. The effect of fracture energy classification (low versus high energy) on liberated surface area was also assessed.

Histologic sections were prepared of the entire knee joints from both hind limbs of all mice. Following formalin-fixation and scanning with microCT, all limbs were decalcified, sequentially dehydrated in ethanol, infiltrated with xylene, and paraffin-embedded. Histology sections (8μm thick) were taken in the coronal plane.

Synovial pathology in the knee following articular fracture was evaluated at day 0 and 7 post-fracture in histologic sections from all limbs without NBT staining (n=5 per group). Due to histology processing issues, one animal from the low energy group was excluded. Two sections in the central and anterior regions were stained with Harris hematoxylin and eosin (H&E). The synovial insertion of the lateral femur, medial femur, lateral tibia, and medial tibia were evaluated separately using a modified form of an established synovitis score [29] (Figure 1) for changes in synovial lining thickness and cellular density in the synovial stroma *(maximum site score 6)* by 4 blinded graders. The correlation between degree of synovitis and applied fracture energy or liberated surface area was also assessed.

To evaluate cartilage pathology of the knee, histologic sections from the central region from all joints at day 0 and 7 post-fracture were stained with Safranin-O and fast green. A modified Mankin histologic scoring system [30, 31] was used to evaluate cartilage pathology and degenerative changes in cartilage structure, proteoglycan staining, tidemark duplication, fibrocartilage, clones, hypertrophic chondrocytes, and subchondral bone thickness [23, 32]. The lateral femur, medial femur, lateral tibia, and medial tibia were graded separately by 4 blinded graders. A total modified Mankin score representing the overall state of the cartilage in the joint was summed from the scores of the individual locations (*maximum score of 120*).

Systemic levels of inflammatory cytokines, hyaluronic acid (HA), and cartilage oligomeric matrix protein (COMP) were measured. For these measures, it was necessary to use non-fractured and shams as controls. At the time of sacrifice, approximately 150μl of blood was collected via retro-orbital bleed followed by a cardiac stick (randomly selected, n=3-4 per group). Collected blood was centrifuged (model IEC Centra CL3R; ThermoScientific; Waltham, MA) at 3500RPM (2450 RCF) for 15min, and the sera were stored at −80°C until analyzed. Inflammatory cytokines were quantified using the Bio-Plex Mouse cytokine 23-Plex Panel multiplex bead assay (Bio-Rad Laboratories, Inc., Hercules, CA), which included IL-1α, IL-1β, IL-4, IL-6, IL-10, and tumor necrosis factor alpha (TNF-α). All samples were analyzed as recommended by the manufacturer using a standard range of 0-3200pg/mL and a sample dilution of 1:2; utilizing a total of 30μL of sera. Commercially available ELISA kits were used for measuring HA (Corgenix, Westminster, CO), and COMP (animal kit; AnaMar, Lund, Sweden) and performed as per the manufacturer's instructions.

Multifactorial analysis of variance (ANOVA) was utilized to examine statistical differences between experimental and control limbs along with the effect of healing time with significance reported at the 95% confidence level (STATISTICA v.7, StatSoft, Inc.). Log transformation was used for data not normally distributed. For synovitis assessment, statistical analysis was performed using nonparametric analyses with significance reported at the 95% confidence level. Statistical analysis for correlations between synovitis and either liberated surface area or applied fracture energy was also performed using nonparametric analyses with significance reported at the 95% confidence interval. Correlations between chondrocyte viability and other measured parameters were performed using regression analysis.

RESULTS

Overall fracture success rate was 95%. Fractures were most commonly located in the lateral aspect of the tibial plateau due to the orientation of the applied load. High energy fractures demonstrated more comminution and displacement of fragments within the tibial plateau (Figure 2). The maximum load was significantly different (p=0.006E-5) between the low (-32±6 N) and high energy (-45±5 N) fractures. The applied energy of fracture was significantly different (p=0.009E-10) between the low (90±33 mJ) and high energy (177±25 mJ) fractures.

Chondrocyte viability, as assessed by a total joint score of cell death, showed no effect of sham procedure (p=0.13; power=0.86). There was no difference in chondrocyte death between low and high energy fractures (p=0.68; power=0.40) (Figure 3A). However, fracture resulted in reduced chondrocyte viability overall with the total joint score of chondrocyte cell death being greater in the experimental limb than the contralateral control limb (p=0.01) in both the anterior and central regions of the knee joint (Figure 3A). In examining the effect of location within the joint, chondrocyte death in the experimental limb was greater than the control limb in the lateral femoral condyle (p=0.003), medial femoral condyle (p=0.04) and lateral aspect of the tibial plateau (p=0.02) (Figure 3B). Additionally, cell death was greater in the lateral tibia than the medial tibia in the experimental limb (p=0.0002) for the anterior region of the knee (Figure 3B). There was also an effect of time on chondrocyte viability, as more cell death occurred at day 7 post-fracture (2.3±1.0) as compared to day 0 (0.8±0.8; p=0.03) and day 1 (0.5±0.5; p=0.04) post-fracture within the lateral aspect of the tibial plateau in the fractured limb.

Morphological bone changes were evident in the fractured limbs (Table 2). Within the tibial plateau (Table 2), all fractures showed a decrease in subchondral bone thickness within seven days of fracture (p=0.02) compared to contralateral control limbs, but no statistically significant difference was found between low and high energy fractures. However, there was a significant decrease in bone density in high energy fractures compared to low energy fractures in the tibial plateau (p=0.05). Within the tibial metaphysis (Table 2), all fractures showed a decrease in bone density compared to control limbs (p=0.003) but no significant difference was found between low and high energy fractures. Within the femoral condyles (Table 2), both bone density (p=0.004) and cancellous bone fraction (p=0.01) was decreased with fracture compared to control limbs, and high energy fractures demonstrated greater decreases in bone density than low energy fractures (p=0.02).

High energy fractures had a greater degree of liberated cortical bone surface area (7.2±2.1 mm^2), indicating greater comminution (Figure 4A), than low energy fractures (3.3±2.0 mm^2; p=0.03). A linear trend (R^2=0.70, p=0.01) between liberated surface area and energy absorbed in fracture was observed (Figure 4B).

For low and high energy fractures, there were no significant differences in synovitis scores between fractured and contralateral control limbs at day 0 (Figure 5). For low energy fractures at day 7, synovitis scores for fractured limbs were significantly higher than the non-fractured control limb at three sites (Figure 5A): the lateral tibia (p=0.043), lateral femur (p=0.043), and medial tibia (p=0.043). Among fractured limbs alone, lateral tibia scores were significantly higher than both medial site scores (medial tibia, p=0.010; and medial femur, p=0.030). For high energy fractures at day 7, synovitis scores for fractured limbs were significantly higher than the non-fractured control limb at all sites (Figure 5B): the lateral tibia (p=0.043), lateral femur (p=0.043), medial tibia (p=0.043), and medial femur (p=0.043). Among fractured limbs alone, lateral tibia scores were significantly higher than only the medial femur site scores (p=0.010). Representative images of the lateral tibia

grading site for contralateral control and fractured experimental limbs 7 days post-fracture are shown (Figure 5B). Applied fracture energy was significantly correlated with synovitis score in the synovial lining layer at the medial tibia only (Spearman correlation, ρ=0.46). There were no other significant correlations between synovitis scores and either applied fracture energy or liberated surface area.

There was no significant difference between modified Mankin scores in the articular cartilage between low and high energy fractures (p=0.22; power= 0.21). Additionally, modified Mankin scores did not reveal any significant difference between fractured experimental and contralateral control limbs at 0 and 7 days post-fracture (day 0, experimental vs. control: 21.3±6.2 vs. 22.6±9.9; day 7 experimental vs. control: 17.8±7.7 vs. 20.8±6.4; p=0.64; power=0.25). However, there was a correlation between Mankin score and chondrocyte death (log(Mankin) vs log(NBT); R^2=0.38, p=0.001). Of the individual components assessed with the Mankin grade, only structural changes within the articular cartilage correlated with increased chondrocyte death (R^2=0.28, p=0.01).

For cartilage and joint-capsule derived biomarkers, serum levels of HA increased significantly at day 1 (p=0.0005) for all fractures and trended upwards at all time points post-fracture, although there was no effect of fracture type (Table 3). Serum levels of COMP also trended upwards at all time points post-fracture but there was no significant difference at any time point (p=0.31; power=0.30) (Table 3). Interestingly, systemic COMP levels did correlate with chondrocyte death (log(COMP) vs log(NBT); R^2= 0.19, p=0.03).

For inflammatory cytokines, there were lower serum levels of IL-1α at day 3 for all fractures, although there was no effect of fracture type (Table 3). There also appeared to be a transient increase in serum levels of IL-1β at day 5 for all fractures (p=0.27; power=0.49) and a decrease in IL-10 at day 7 for high energy fractures (p=0.14; power=0.41), although these trends were not significant (Table 3). For the other inflammatory cytokines evaluated, there was no significant effect of fracture or fracture severity on serum levels at any time point after fracture.

DISCUSSION

This study demonstrates that in a closed intra-articular fracture in the mouse knee, increasing energy of fracture was associated with greater acute pathology in the bone and synovium and with increasing comminution compared to control limbs. These changes included increased synovitis throughout the entire joint and greater changes in bone morphology. Both low and high energy fractures were associated with lateral joint pathology, but only high energy fractures resulted in inflammation medially, with higher energy fractures demonstrating more global joint synovitis. The applied energy of fracture was significantly correlated with degree of liberated cortical bone surface area, indicating greater comminution. Fracture of the articular surface significantly increased serum concentrations of HA one day after fracture. While the presence of an articular fracture significantly reduced chondrocyte viability, there was no relationship between increasing fracture severity and chondrocyte viability, cartilage pathology, or systemic levels of cytokines and biomarkers, at least in the acute setting after articular fracture examined in this study.

Although the direct mechanisms linking traumatic joint injury and the development of PTA are not well understood, intra-articular fractures are commonly associated with development of the disease, and clinical outcomes are closely linked to the severity of trauma and subsequent degeneration of the articular cartilage [2]. Clinically, more complex intra-articular fractures are associated with higher energy injuries, and patients with more

complex articular injuries had a worse outcomes [3]. The severity of comminution may play the greatest role in the long-term functionality of the joint after trauma [23]. Our data suggest that fracture severity is significantly associated with increased pathology in the synovium and bone in the joint. These findings support an “organ-level” conceptualization of the joint as most appropriate in regard to its response to injury, as trauma to one type of joint tissue may lead to acute pathology in another through various mechanisms. For example, a recent *in vitro* co-culture study showed that mechanical injury to cartilage in the presence of joint capsule tissue explants shifted chondrocyte metabolism towards pro-catabolic pathways that may result in matrix degradation [33]. Several researchers now propose that processes affecting either cartilage, bone, or synovium eventually intertwine and collectively damage all three components as well [34-36]. In the acute 7-day period of our study minimal changes in cartilage pathology was observed, but increasing injury to the articular surface appears to result in greater synovitis, which may contribute to long-term dysregulation of chondrocyte function and lead to degenerative changes in the articular cartilage characteristic of PTA. Further characterization of the early events following trauma and an improved understanding of their interrelationships could aid in the treatment and prevention of PTA following articular fracture.

In order to assess regional variation in chondrocyte viability through the depth of the cartilage, a cross-section of the articular cartilage was needed. For confocal microscopy, this required bisecting the joint in the coronal plane to obtain a cross-sectional view of the articular cartilage. This was technically challenging because of the small size and instability of the fractured mouse knee joint resulted in disruption of the articular surface. As an alternative to a fluorescent live/dead assay with confocal microscopy, chondrocyte viability was assessed using NBT. NBT is cell-permeable and metabolized by live cells to form a blue formazan product which remains stable to standard histological preparation and paraffin-embedding. A possible limitation of NBT is that cell death may be overestimated because live cells with altered metabolic activity may be counted as dead cells. However, Lewis et al. showed excellent correlation between NBT and confocal microscopy with a live/dead assay for the assessment chondrocyte viability in traumatically impacted cartilage [26, 27].

This model uses an “organ-level” approach to study joint injury. By utilizing a closed-joint model, a limitation is that the specific stresses and strains on the cartilage are not known. In this model, the initial aspects of loading are similar between the two groups. However, our data demonstrated a significant correlation between applied fracture energy and degree of cortical bone liberated surface area. These injury severity measures differed significantly between the two groups. Previous investigators have characterized this relationship using a drop-tower and a uniform sample of bovine bone from the midshaft of the tibia [4]. This concept of determining liberated surface area has been applied to fractures of the distal tibia in humans as a method of determining injury severity [37]. Despite having a closed-joint, *in vivo* model of fracture and a relatively small sample size, our results demonstrated similar trends in the relationship between liberated surface area and applied load. In both these models, high energy fractures resulted in more comminution compared to low energy fractures. These results indicate that our closed-joint, *in vivo* model results in fractures that can be controlled by the load-displacement profile and is consistent with other clinical measures of joint fracture severity described in the literature [4, 37]. As the technique of determining liberated surface area via microCT is time intensive, these results indicate that, for future studies, the use of energy of fracture is an appropriate measure of injury severity in place of liberated surface area.

MicroCT analysis revealed decreased bone density with fracture in the femoral condyles, tibial plateau and metaphysis. These trends were similar to those observed in the pilot study

of this mouse model [38]. There was also a significant decrease in subchondral bone thickness over the course of seven days. This loss of subchondral bone along with decreased bone density following fracture may be analogous to periarticular bone loss associated with inflammation and active synovitis in early rheumatoid arthritis [39, 40]. Disuse of the injured limb may also contribute to bone loss. However, this mechanism of bone loss may be unlikely as limb immobilization models in the mouse only show significant decreases in bone after 10 days of immobilization [41]. Further work is needed to understand the significance of this early bone resorption.

Chondrocyte viability was significantly affected by proximity to the fracture site, with the greatest cell death occurring in the lateral aspect of the tibial plateau, corresponding to the location of most fractures. Chondrocyte death also significantly increased, however, in the lateral and medial femoral condyles compared to the contralateral control limb, indicating a complex response by all articular surfaces of the joint. Although fractures were initiated from an anterior approach, anterior and central regions within the joint demonstrated similar levels of chondrocyte death. Chondrocyte death in experimental limbs also increased with time. The delay to maximal cell death is similar to trends observed in human cartilage after traumatic joint injury that may implicate apoptosis in chondrocyte death [42]. In addition, this time frame is consistent with previous studies and may suggest that some chondrocytes undergo immediate necrosis while others progress through the apoptotic pathway and die several days after injury [43-46]. However, the chondrocyte viability assay used in this study precluded subsequent determination of apoptosis, and thus it is unclear whether cell death can be attributed specifically to necrosis or apoptosis. Future investigations might further address this issue.

Biomarkers such as HA or COMP are useful indicators of cellular processes and presumably, the severity of joint disease by minimally invasive means [47-49]. Serum levels of HA increased significantly on day 1 after both high and low energy fractures. Both serum HA and COMP have been shown to predict disease outcome in knee [50] and hip OA [51] and to correlate with OA progression [50-56] in humans. Further identification of the roles of these and other novel biomarkers in future studies may provide powerful tools for the measurement of disease severity in PTA.

This study demonstrates that increased severity of closed articular fracture in the mouse knee is significantly associated with increased synovitis throughout the joint, increased degree of cortical bone fragmentation, and greater bone morphometric changes. We have also shown that fracture of the articular surface is associated with significantly increased cell death and transient increases in HA and COMP. The precise role of acute pathology in various joint tissues following fracture in the ultimate progression to PTA remains unknown. Further characterization of the early events following trauma could aid in the treatment and prevention of PTA following articular fracture.

Acknowledgments

We would like to recognize Steve Johnson for his excellent technical support. This work was supported by a Howard Hughes Medical Fellowship, Piedmont Orthopedic Foundation Resident Research grant, and NIH grants AR50245, AG15768, AR48182, AR48852, and AR055659.

References

1. Swiontkowski MF, Chapman JR. Cost and effectiveness issues in care of injured patients. Clinical Orthopaedics & Related Research. 1995:17–24. [PubMed: 7671513]

2. Brown TD, Johnston RC, Saltzman CL, Marsh JL, Buckwalter JA. Post-Traumatic Osteoarthritis: A First Estimate of Incidence, Prevalence, and Burden of Disease. Journal of Orthopaedic Trauma. 2006; 20:739–44. [PubMed: 17106388]
3. Swiontkowski MF, Agel J, McAndrew MP, Burgess AR, MacKenzie EJ. Outcome validation of the AO/OTA fracture classification system. J Orthop Trauma. 2000; 14:534–41. [PubMed: 11149498]
4. Beardsley CL, Anderson DD, Marsh JL, Brown TD. Interfragmentary surface area as an index of comminution severity in cortical bone impact. J Orthop Res. 2005; 23:686–90. [PubMed: 15885492]
5. Lovasz G, Llinas A, Benya PD, Park SH, Sarmiento A, Luck JV Jr. Cartilage changes caused by a coronal surface stepoff in a rabbit model. Clin Orthop Relat Res. 1998:224–34. [PubMed: 9755783]
6. Llinas A, McKellop HA, Marshall GJ, Sharpe F, Kirchen M, Sarmiento A. Healing and remodeling of articular incongruities in a rabbit fracture model. J Bone Joint Surg Am. 1993; 75:1508–23. [PubMed: 8408140]
7. Lefkoe T, Walsh WR, et al. Remodeling of Articular Step-Offs. Clinical Orthopaedics & Related Research. 1995; 314:253–65. [PubMed: 7634643]
8. Delamarter RB, Hohl M, Hopp E Jr. Ligament injuries associated with tibial plateau fractures. Clin Orthop Relat Res. 1990:226–33. [PubMed: 2293934]
9. Lansinger O, Bergman B, Korner L, Andersson GB. Tibial condylar fractures. A twenty-year follow-up. J Bone Joint Surg Am. 1986; 68:13–9. [PubMed: 3941115]
10. Kamekura S, Hoshi K, Shimoaka T, Chung U, Chikuda H, Yamada T, et al. Osteoarthritis development in novel experimental mouse models induced by knee joint instability. Osteoarthritis Cartilage. 2005; 13:632–41. [PubMed: 15896985]
11. Torzilli PA, Grigiene R, Borrelli J Jr, Helfet DL. Effect of impact load on articular cartilage: Cell metabolism and viability, and matrix water content. Journal of Biomechanical Engineering. 1999; 121:433–41. [PubMed: 10529909]
12. Ewers BJ, Dvoracek-Driksna D, Orth MW, Haut RC. The extent of matrix damage and chondrocyte death in mechanically traumatized articular cartilage explants depends on rate of loading. J Orthop Res. 2001; 19:779–84. [PubMed: 11562121]
13. Donohue JM, Buss D, Oegema TR Jr, Thompson RC Jr. The effects of indirect blunt trauma on adult canine articular cartilage. J Bone Joint Surg Am. 1983; 65:948–57. [PubMed: 6885875]
14. Thompson RC Jr, Oegema TR Jr, Lewis JL, Wallace L. Osteoarthrotic changes after acute transarticular load. An animal model. Journal of Bone & Joint Surgery - American Volume. 1991; 73:990–1001.
15. Borrelli J Jr, Zhu Y, Burns M, Sandell L, Silva MJ. Cartilage tolerates single impact loads of as much as half the joint fracture threshold. Clin Orthop Relat Res. 2004:266–73. [PubMed: 15346084]
16. Loening AM, James IE, Levenston ME, Badger AM, Frank EH, Kurz B, et al. Injurious mechanical compression of bovine articular cartilage induces chondrocyte apoptosis. Arch Biochem Biophys. 2000; 381:205–12. [PubMed: 11032407]
17. Blanco FJ, Guitian R, Vazquez-Martul E, de Toro FJ, Galdo F. Osteoarthritis chondrocytes die by apoptosis. A possible pathway for osteoarthritis pathology. Arthritis Rheum. 1998; 41:284–9. [PubMed: 9485086]
18. D'Lima D, Hashimoto S, Chen P, Colwell CJ, Lotz M. Impact of mechanical trauma on matrix and cells. Clinical Orthopaedics & Related Research. 2001; 391(Suppl)
19. Fernandes J, Martel-Pelletier J, Pelletier J. The role of cytokines in osteoarthritis pathophysiology. Biorheology. 2002; 39:237. [PubMed: 12082286]
20. Goldring MB. Osteoarthritis and cartilage: the role of cytokines. Curr Rheumatol Rep. 2000; 2:459–65. [PubMed: 11123098]
21. Benito MJ, Veale DJ, FitzGerald O, van den Berg WB, Bresnihan B. Synovial tissue inflammation in early and late osteoarthritis. Ann Rheum Dis. 2005; 64:1263–7. [PubMed: 15731292]
22. Smeets TJ, Kraan MC, van Loon ME, Tak PP. Tumor necrosis factor alpha blockade reduces the synovial cell infiltrate early after initiation of treatment, but apparently not by induction of apoptosis in synovial tissue. Arthritis Rheum. 2003; 48:2155–62. [PubMed: 12905468]

23. Furman BD, Strand J, Hembree WC, Ward BD, Guilak F, Olson SA. Joint degeneration following closed intraarticular fracture in the mouse knee: A model of posttraumatic arthritis. Journal of Orthopaedic Research. 2007; 25:578–92. [PubMed: 17266145]
24. Beamer WG, Donahue LR, Rosen CJ, Baylink DJ. Genetic variability in adult bone density among inbred strains of mice. Bone. 1996; 18:397–403. [PubMed: 8739896]
25. Sheng MH-C, Baylink DJ, Beamer WG, Donahue LR, Rosen CJ, Lau K-HW, et al. Histomorphometric studies show that bone formation and bone mineral apposition rates are greater in C3H/HeJ (high-density) than C57BL/6J (low-density) mice during growth. Bone. 1999; 25:421–29. [PubMed: 10511108]
26. Lazarus B, Messina A, Barker JE, Hurley JV, Romeo R, Morrison WA, et al. The role of mast cells in ischaemia-reperfusion injury in murine skeletal muscle. The Journal of Pathology. 2000; 191:443–48. [PubMed: 10918220]
27. Lewis JL, Deloria LB, Oyen-Tiesma M, Thompson J, Roby C, Ericson M, Oegema J, Theodore R. Cell death after cartilage impact occurs around matrix cracks. Journal of Orthopaedic Research. 2003; 21:881–87. [PubMed: 12919877]
28. Caputo AM, Lee JY, Spritzer CE, Easley ME, DeOrio JK, Nunley JA 2nd, et al. In vivo kinematics of the tibiotalar joint after lateral ankle instability. Am J Sports Med. 2009; 37:2241–8. [PubMed: 19622791]
29. Krenn V, Morawietz L, Burmester GR, Kinne RW, Mueller-Ladner U, Muller B, et al. Synovitis score: discrimination between chronic low-grade and high-grade synovitis. Histopathology. 2006; 49:358–64. [PubMed: 16978198]
30. Carlson CS, Guilak F, Vail TP, Gardin JF, Kraus VB. Synovial fluid biomarker levels predict articular cartilage damage following complete medial meniscectomy in the canine knee. Journal of Orthopaedic Research. 2002; 20:92–100. [PubMed: 11853096]
31. Mankin H, Dorfman H, Lippiello L, Zarins A. Biochemical and metabolic abnormalities in articular cartilage from osteoarthritic human hips. II. Correlation of morphology with biochemical and metabolic data. J Bone Joint Surg Am. 1971; 53:523–37. [PubMed: 5580011]
32. Bulstra S, Buurman WA, Walenkamp GH, van der Linden AJ. Metabolic characteristics of in vitro cultured human chondrocytes in relation to the histopathologic grade of osteoarthritis. Clinical Orthopaedics & Related Research. 1989; 242:294–302. [PubMed: 2706860]
33. Lee JH, Fitzgerald JB, DiMicco MA, Cheng DM, Flannery CR, Sandy JD, et al. Co-culture of mechanically injured cartilage with joint capsule tissue alters chondrocyte expression patterns and increases ADAMTS5.production. Arch Biochem Biophys. 2009; 489:118–26. [PubMed: 19607802]
34. Goldring MB. Update on the biology of the chondrocyte and new approaches to treating cartilage diseases. Concepts of pathogenesis and emerging treatments for rheumatic diseases. 2006; 20:1003–25.
35. Krasnokutsky S, Samuels J, Abramson SB. Osteoarthritis in 2007. Bull NYU Hosp Jt Dis. 2007; 65:222–8. [PubMed: 17922674]
36. Attur M, Samuels J, Krasnokutsky S, Abramson SB. Targeting the synovial tissue for treating osteoarthritis (OA): where is the evidence? Best Pract Res Clin Rheumatol. 2010; 24:71–9. [PubMed: 20129201]
37. Anderson DD, Mosqueda T, Thomas T, Hermanson EL, Brown TD, Marsh JL. Quantifying tibial plafond fracture severity: Absorbed energy and fragment displacement agree with clinical rank ordering. Journal of Orthopaedic Research. 2008; 26:1046–52. [PubMed: 18327811]
38. Furman BD, Olson SA, Guilak F. The development of posttraumatic arthritis after articular fracture. J Orthop Trauma. 2006; 20:719–25. [PubMed: 17106385]
39. Green MJ, Deodhar AA. Bone changes in early rheumatoid arthritis. Best Pract Res Clin Rheumatol. 2001; 15:105–23. [PubMed: 11358418]
40. Shimizu S, Shiozawa S, Shiozawa K, Imura S, Fujita T. Quantitative histologic studies on the pathogenesis of periarticular osteoporosis in rheumatoid arthritis. Arthritis Rheum. 1985; 28:25–31. [PubMed: 3966938]

41. Rantakokko J, Uusitalo H, Jamsa T, Tuukkanen J, Aro HT, Vuorio E. Expression profiles of mRNAs for osteoblast and osteoclast proteins as indicators of bone loss in mouse immobilization osteopenia model. J Bone Miner Res. 1999; 14:1934–42. [PubMed: 10571694]

42. Hembree WC, Ward BD, Furman BD, Zura RD, Nichols LA, Guilak F, et al. Viability and apoptosis of human chondrocytes in osteochondral fragments following joint trauma. J Bone Joint Surg Br. 2007; 89:1388–95. [PubMed: 17957084]

43. Kim HT, Lo MY, Pillarisetty R. Chondrocyte apoptosis following intraarticular fracture in humans. Osteoarthritis Cartilage. 2002; 10:747–9. [PubMed: 12202127]

44. Murray MM, Zurakowski D, Vrahas MS. The death of articular chondrocytes after intra-articular fracture in humans. J Trauma. 2004; 56:128–31. [PubMed: 14749579]

45. Tew SR, Kwan AP, Hann A, Thomson BM, Archer CW. The reactions of articular cartilage to experimental wounding: role of apoptosis. Arthritis Rheum. 2000; 43:215–25. [PubMed: 10643718]

46. D'Lima DD, Hashimoto S, Chen PC, Colwell J, C W, Lotz MK. Human chondrocyte apoptosis in response to mechanical injury. Osteoarthritis and Cartilage. 2001; 9:712–19. [PubMed: 11795990]

47. Saxne T, Heinegard D. Synovial fluid analysis of two groups of proteoglycan epitopes distinguishes early and late cartilage lesions. Arthitis Rheum. 1992; 35:385–90.

48. Hazell PK, Dent C, Fairclough JA, Bayliss MT, Hardingham TE. Changes in glycosaminoglycan epitope levels in knee joint fluid following injury. Arthritis & Rheumatism. 1995; 38:953–9. [PubMed: 7541993]

49. Lindhorst E, Vail TP, Guilak F, Wang H, Setton LA, Vilim V, et al. Longitudinal characterization of synovial fluid biomarkers in the canine meniscectomy model of osteoarthritis. Journal of Orthopaedic Research. 2000; 18:269–80. [PubMed: 10815829]

50. Sharif M, George E, Shepstone L, Knudson W, Thonar EJ, Cushnaghan J, et al. Serum hyaluronic acid level as a predictor of disease progression in osteoarthritis of the knee. Arthritis & Rheumatism. 1995; 38:760–7. [PubMed: 7779118]

51. Mazieres B, Garnero P, Gueguen A, Abbal M, Berdah L, Lequesne M, et al. Molecular markers of cartilage breakdown and synovitis at baseline as predictors of structural progression of hip osteoarthritis. The ECHODIAH Cohort. Ann Rheum Dis. 2006; 65:354–59. [PubMed: 16322084]

52. Otterness IG, Swindell AC, Zimmerer RO, Poole AR, Ionescu M, Weiner E. An analysis of 14 molecular markers for monitoring osteoarthritis: segregation of the markers into clusters and distinguishing osteoarthritis at baseline. Osteoarthritis & Cartilage. 2000; 8:180–5. [PubMed: 10806045]

53. Garnero P, Piperno M, Gineyts E, Christgau S, Delmas PD, Vignon E. Cross sectional evaluation of biochemical markers of bone, cartilage, and synovial tissue metabolism in patients with knee osteoarthritis: relations with disease activity and joint damage. Ann Rheum Dis. 2001; 60:619–26. [PubMed: 11350852]

54. Pavelka K, Forejtová S, Olejárová M, Gatterová J, Senolt L, Spaek P, et al. Hyaluronic acid levels may have predictive value for the progression of knee osteoarthritis. Osteoarthritis & Cartilage. 2004; 12:277. [PubMed: 15023379]

55. Bruyere O, Collette J, Kothari M, Zaim S, White D, Genant H, et al. Osteoarthritis, magnetic resonance imaging, and biochemical markers: a one year prospective study. Ann Rheum Dis. 2006; 65:1050–54. [PubMed: 16396978]

56. Jung YO, Do JH, Kang HJ, Yoo SA, Yoon CH, Kim HA, et al. Correlation of sonographic severity with biochemical markers of synovium and cartilage in knee osteoarthritis patients. Clin Exp Rheumatol. 2006; 24:253–9. [PubMed: 16870091]

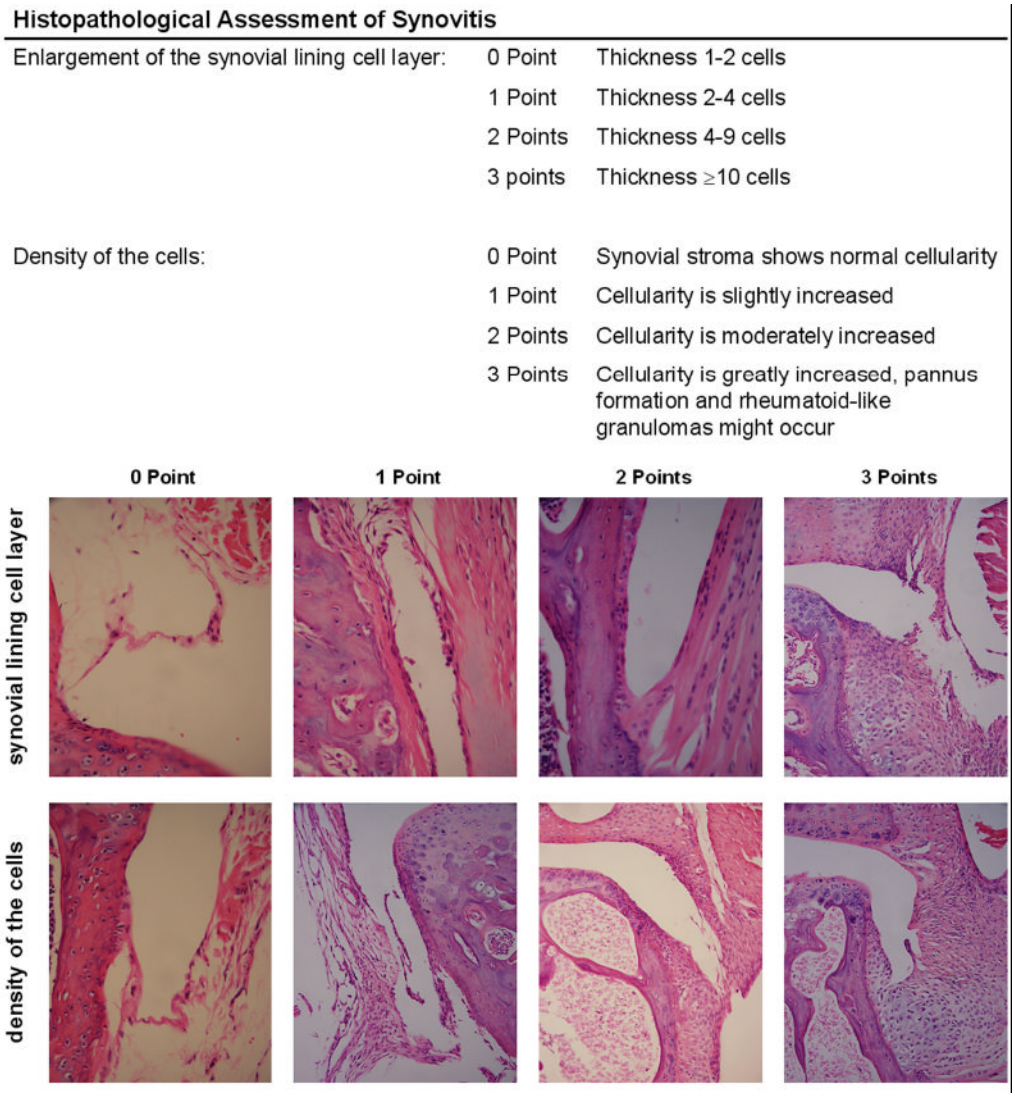

Figure 1.

Histopathological assessment of synovitis (modified from Krenn et al. Histopathology 2006). Enlargement of the synovial lining cell layer and density of the cells in the synovial stroma were individually assessed from H&E histology sections of mouse knee joints (magnification 100-200×).

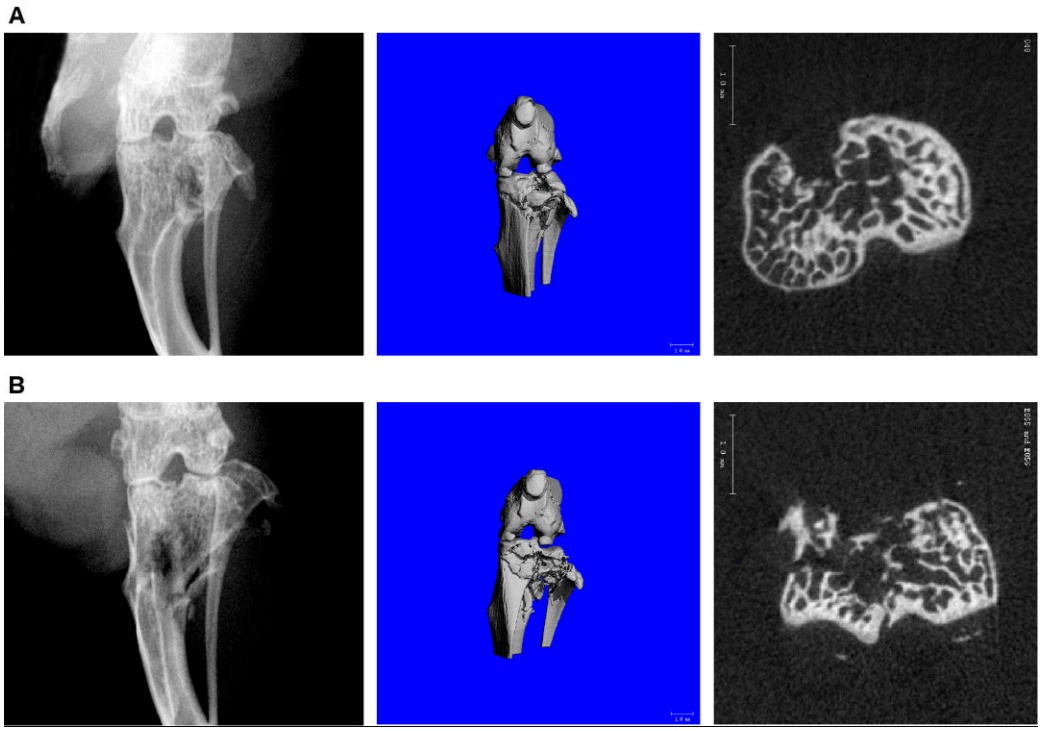

Figure 2.
Low energy (A) and high energy (B) fractures of the mouse tibial plateau. Radiograph (left), micro computed tomography (microCT) three-dimensional rendered image (middle, scale bar = 1mm), and microCT cross-section (right, scale bar = 1mm) demonstrating joint morphology of fractures at t=0 day post-fracture.

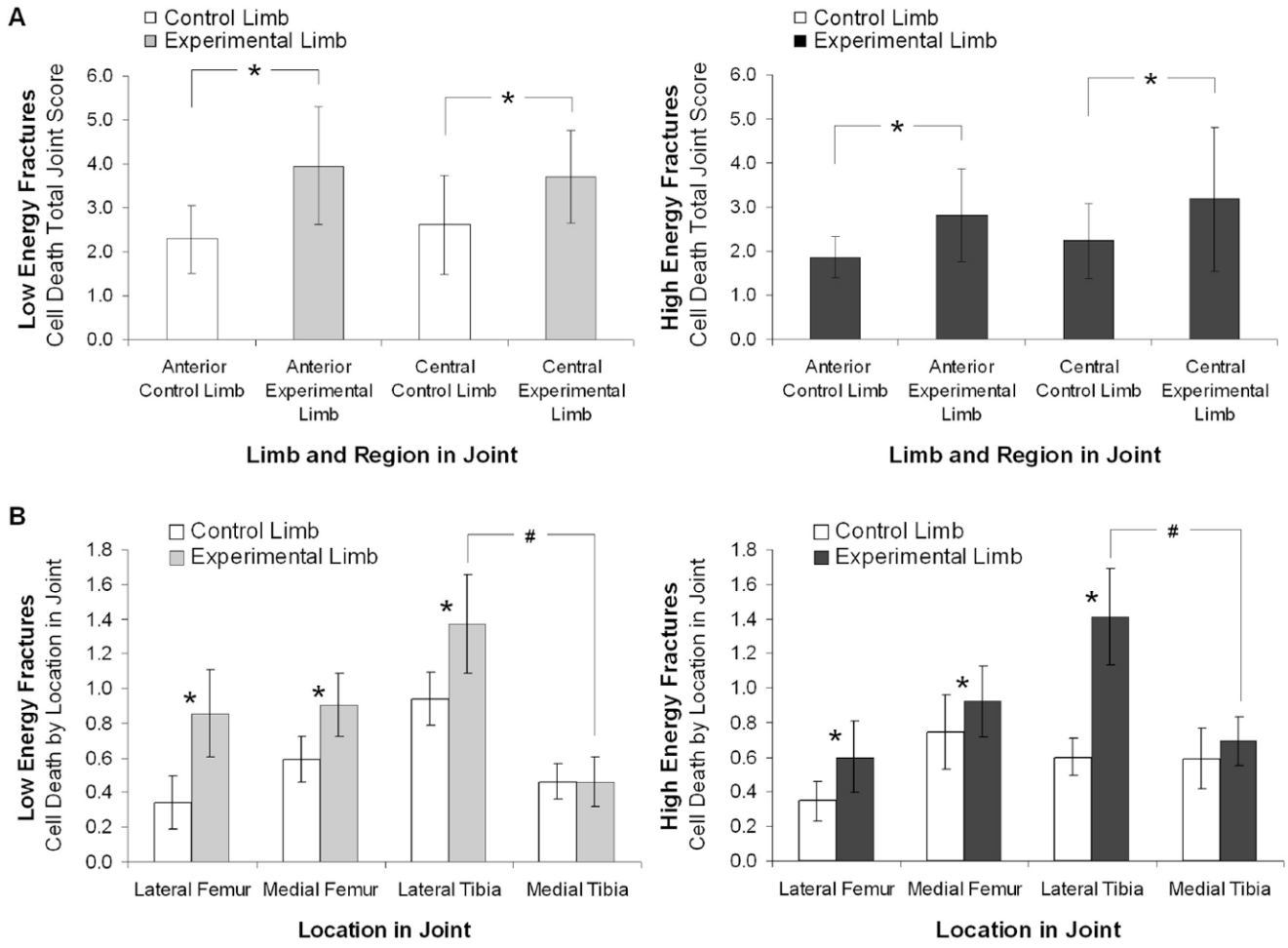

Figure 3.

Chondrocyte cell death as assessed by NBT nuclear stain (n=3 per group per timepoint). Vertical bars denote ± 95% CI. A. The total joint score *(maximum possible total joint score = 20)* of cell death was greater in the fractured experimental limb than the contralateral control limb in both the anterior and central regions of the knee joint (*p=0.014 for anterior region, p=0.016 for central region). B. Cell death by location in the joint *(maximum possible site score = 5)* was greater in the fractured experimental limb than the contralateral control limb (* p=0.003 for lateral femur, p=0.04 for medial femur, p=0.001 for lateral tibia), and cell death was significantly greater in the lateral tibial than the medial tibia in the fractured experimental limb (p=0.0002) for the anterior region of the knee. For all measures of chondrocyte cell death there was no significant difference between low energy and high energy fractures.

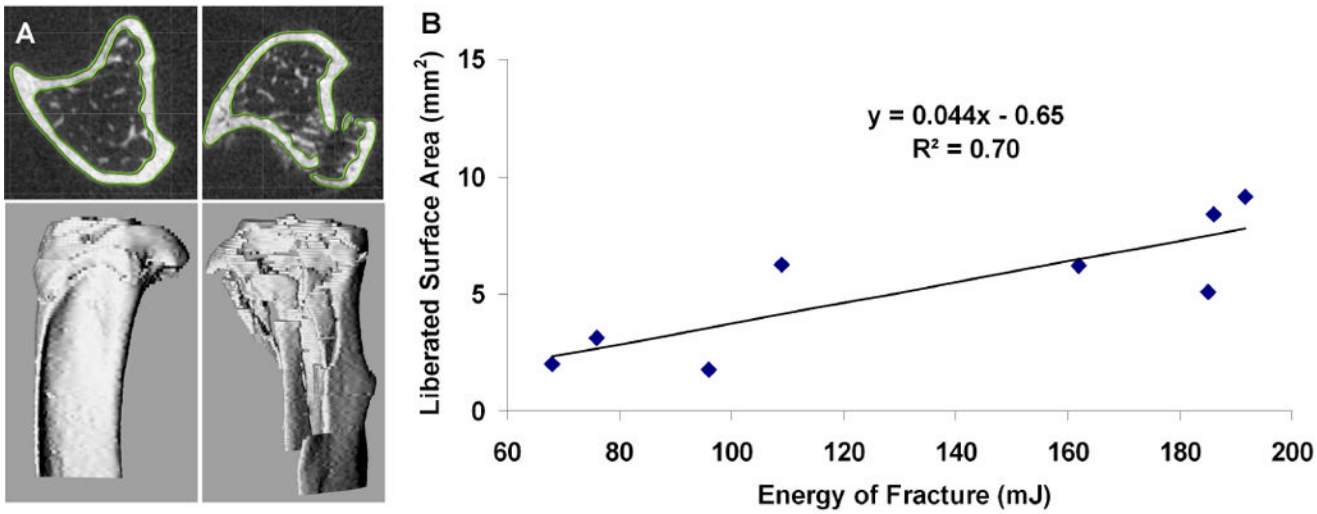

Figure 4.

A. MicroCT images were segmented using a semi-automated custom software in both the intact contralateral control limb (left) and fractured experimental limb (right). These models were then registered to each other using an iterative closest point technique, and were used to calculate liberated surface area. B. Fracture severity, as measured from the liberated surface area, was well correlated to the energy of fracture, as calculated from the load-displacement data (R^2=0.70).

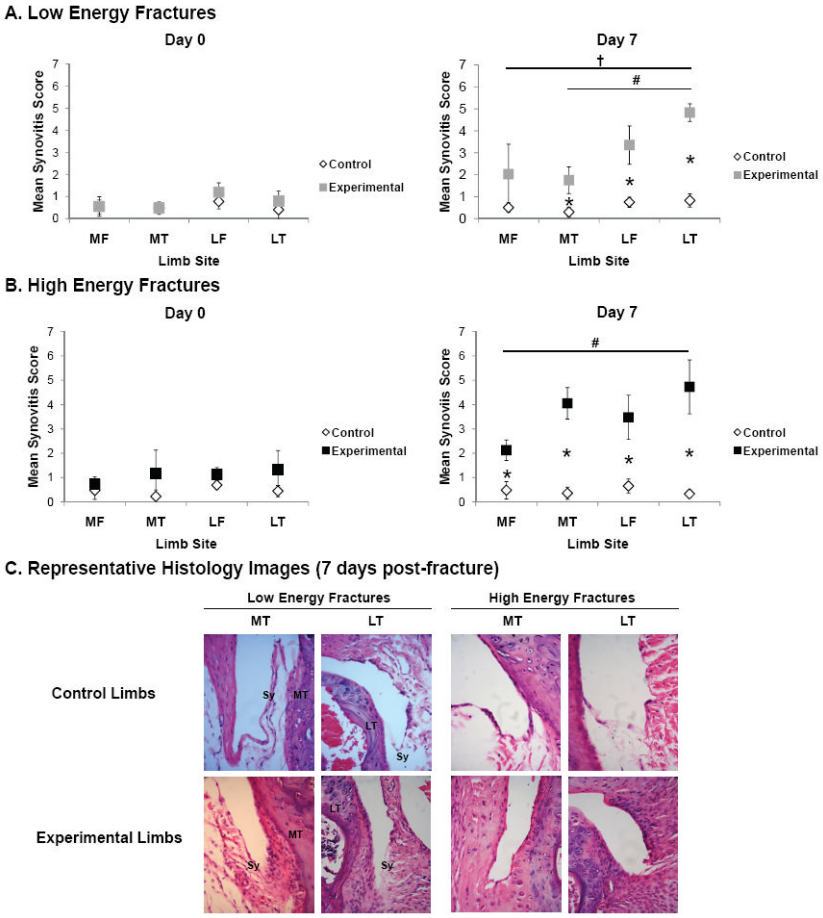

Figure 5.

Assessment of synovitis in low and high energy fractures (n=5 per group per timepoint). A. Synovitis scores at 0 and 7 days post-fracture. Vertical bars denote ± 95% CI. B. Representative histologic sections of the synovial insertion (Sy) at the medial tibia (MT) and lateral tibia (LT) in contralateral control and fractured experimental limbs at 7 days post-fracture (H&E stain; 400× magnification).

Table 1

Grading scheme for assessment of chondrocyte viability in the mouse knee joint from nitroblue tetrazolium (NBT) staining in viable cells. Maximum possible site score of 5 for the medial and lateral femoral condyles and tibial plateau. Maximum possible total joint score of 20 summed from site scores for each joint.

Grade	Description
0	≥ 95% viable cells in all of plateau or condyle
1	cell death in < ½ plateau or condyle, < ½ depth
2	cell death in < ½ plateau or condyle, ≥ ½ depth
3	cell death in ≥ ½ plateau or condyle, < ½ depth
4	cell death in ≥ ½ plateau or condyle, ≥ ½ depth
5	< 10% viable cells in all of plateau or condyle

Table 2

Bone morphometry parameters as assessed by microCT for the tibial plateau, tibial metaphysis, and femoral condyles (mean ± 95% CI).

		Low Energy Fractures		High Energy Fractures	
		t=0 (days)	t=7 (days)	t=0 (days)	t=7 (days)
Tibial Plateau					
Subchondral Thickness (μm)*	Control limb	160 ± 19 [a,b]	182 ± 27 [a]	152 ± 19 [a,b]	168 ± 29 [a]
	Experimental limb	151 ± 15 [a]	137 ± 17 [b]	147 ± 18 [a]	138 ± 15 [b]
Bone Density (mg/cm^3)#	Control limb	1058 ± 24	1063 ± 41	1047 ± 18	1045 ± 30
	Experimental limb	1054 ± 15	1042 ± 30	1034 ± 16	1036 ± 34
Tibial Metaphysis					
Bone Density (mg/cm^3) †	Control limb	971 ± 25	982 ± 20	967 ± 30	964 ± 42
	Experimental limb	930 ± 26	960 ± 34	949 ± 16	942 ± 50
Femoral Condyles					
Bone Density (mg/cm^3) ‡	Control limb	1058 ± 14 [a]	1061 ± 16 [a]	1049 ± 17 [a]	1055 ± 17 [a]
	Experimental limb	1053 ± 15 [a]	1045 ± 21 [b]	1037 ± 9 [a]	1028 ± 14 [c]
Cancellous bone fraction*	Control limb	0.75 ± 0.04 [a]	0.74 ± 0.06 [a]	0.74 ± 0.03 [a]	0.75 ± 0.03 [a]
	Experimental limb	0.72 ± 0.05 [a]	0.63 ± 0.08 [b]	0.69 ± 0.05 [a]	0.59 ± 0.08 [b]

*Indicates significant difference by limb at day 7;

#indicates significant difference by limb and fracture energy

†Indicates significant difference by limb;

‡indicates significant difference by limb and fracture energy at day 7

Post-hoc analysis: values with different letters are significantly different from one another ($p<0.05$).

Table 3

Circulating serum levels of biomarkers and cytokines (n=3-4 per group per timepoint; mean ± 95% CI).

		Pre-Fx	Post-Fx Day 0	Post-Fx Day 1	Post-Fx Day 3	Post-Fx Day 5	Post-Fx Day 7	Sham Day 7
Biomarkers (ng/mL)								
HA*	Non-Fractured	501 ± 291 [a,b]						319 ± 134 [a,b]
	Low Energy Fracture		405 ± 91 [a,b]	1078 ± 4932 [c]	465 ± 538 [b]	601 ± 203 [c]	652 ± 170 [c]	
	High Energy Fracture		352 ± 205 [a,b]	1486 ± 9302 [c]	5355 ± 2869 [b]	639 ± 432 [c]	717 ± 344 [c]	
COMP	Non-Fractured	206 ± 86						223 ± 74
	Low Energy Fracture		223 ± 67	247 ± 784	252 ± 368	231 ± 94	295 ± 90	
	High Energy Fracture		258 ± 70	304 ± 483	259 ± 94	253 ± 367	311 ± 1057	
Pro-Inflammatory Cytokines (pg/mL)								
IL-1α*	Non-Fractured	143 ± 57 [a]						88 ± 72 [a]
	Low Energy Fracture		142 ± 111 [a]	91 ± 474	47 ± 341 b	162 ± 29	93 ± 76	
	High Energy Fracture		258 ± 70 [a]	304 ± 483	259 ± 94 [b]	253 ± 367	311 ± 1057	
IL-1β	Non-Fractured	64 ± 33						60 ± 40
	Low Energy Fracture		82 ± 24	76 ± 459	53 ± 50	232 ± 454	87 ± 59	
	High Energy Fracture		69 ± 31	72 ± 183	75 ± 229	183 ± 509	101 ± 553	
TNF-α	Non-Fractured	568 ± 523						611 ± 871
	Low Energy Fracture		1278 ± 885	1455 ± 14848	704 ± 2128	4033 ± 11448	1218 ± 1796	
	High Energy Fracture		1243 ± 1857	815 ± 3639	957 ± 1769	979 ± 1427	1076 ± 6496	
IL-6	Non-Fractured	84 ± 195						20 ± 25
	Low Energy Fracture		36 ± 18	65 ± 683	105 ± 1120	108 ± 283	23 ± 23	
	High Energy Fracture		31 ± 24	36 ± 71	49 ± 358	27 ± 37	30 ± 118	
Anti-Inflammatory Cytokines (pg/mL)								
IL-4	Non-Fractured	1.19 ± 0.72						0.87 ± 0.59
	Low Energy Fracture		1.45 ± 0.22	1.69 ± 14.55	0.66 ± 0.19	1.51 ± 1.17	1.07 ± 1.33	
	High Energy Fracture		1.27 ± 1.02	1.55 ± 4.07	1.26 ± 0.13	1.29 ± 1.45	1.78 ± 12.58	
IL-10	Non-Fractured	59 ± 39						48 ± 64

	Pre-Fx	Post-Fx Day 0	Post-Fx Day 1	Post-Fx Day 3	Post-Fx Day 5	Post-Fx Day 7	Sham Day 7
Low Energy Fracture		83 ± 74	159 ± 1630	70 ± 131	124 ± 161	63 ± 27	
High Energy Fracture		65 ± 95	97 ± 242	60 ± 4	58 ± 82	40 ± 478	

*Values with different letters are significantly different from one another ($p<0.05$).